Direct Power Control of PWM Rectifiers With Online Inductance Identification Under Unbalanced and Distorted Network Conditions

Yongchang Zhang, *Senior Member, IEEE*, Jian Jiao, and Jie Liu

***Abstract*—In the conventional direct power control (DPC) methods, the grid currents are highly distorted, and substantial ripple is present in the dc-bus voltage under unbalanced and distorted grid conditions. Various improved DPC methods have been proposed to address these problems, but these methods are generally complicated and not easy to use because of the complex controlling structures, need for considerable tuning, and so on. This paper proposes an improved DPC method obtained by simply adding a compensation term to the original power references. The compensation power is obtained by analyzing the power ripple in the input line inductance based on extended power theory. The reference voltage vector is subsequently calculated from the new power reference and synthesized by space vector modulation. To improve the robustness of the proposed DPC against inductance variations, an online inductance identification technique based on the gradient correction method is proposed and combined with the proposed DPC. The presented simulation and experimental results demonstrate that the proposed method can achieve sinusoidal grid currents and significantly reduce the dc-voltage ripple even with mismatched inductance under unbalanced and distorted grid conditions.**

***Index Terms*—DC-link voltage oscillation elimination, inductance identification, power compensation, unbalanced and distorted grid.**

I. Introduction

A THREE-PHASE pulsewidth modulation (PWM) rectifier can achieve sinusoidal grid currents, a constant dc-bus voltage, and a controllable power factor. To date, PWM rectifiers have been widely used in industrial applications, such as ac motor drives with regenerative requirements [1], distributed generation based on renewable energy [2], microgrids [3], HVdc transmissions [4], and so on.

Among the various control methods for PWM rectifiers, direct power control (DPC) has received considerable attention from both industry and academia [5]–[7]. Compared to the popular

Manuscript received September 10, 2018; revised January 31, 2019; accepted March 29, 2019. Date of publication April 1, 2019; date of current version September 6, 2019. This work was supported in part by the National Natural Science Foundation of China under Grant 51577003. Recommended for publication by Associate Editor A. Mertens. *(Corresponding author: Yongchang Zhang.)*

Y. Zhang is with Inverter Technologies Engineering Research Center of Beijing, and the Collaborative Innovation Center of Key Power Energy-Saving Technologies in Beijing, North China University of Technology, Beijing 100144, China (e-mail:

frame transformation. An improved deadbeat control method under unbalanced and distorted grid voltages is proposed in [20]. The deadbeat current control is simple and effective, but the reference current value calculated by the active negative sequence current injection method is complicated because of the requirement of a notch filter, PLL, and reference frame transformation.

During the operation, the actual inductance may vary with the temperature or conducting current. The control performance of many control methods of the three-phase PWM rectifier depends on the mathematical model of the three-phase PWM rectifier, especially model predictive control (MPC) or the deadbeat DPC control method. The control performance will be downgraded if the inductance value in the controller and its actual value are mismatched. Different parameter identification methods are combined with predictive power control on the converters in some papers. In [21], the least squares method is applied to the MPC. The control performance of the PWM rectifier is improved, but the method is conducted only under balanced grid conditions. In [22], an adaptive voltage-oriented control with resistance and inductance estimation is proposed for a PWM rectifier. Although the robustness of the control system is improved, substantial tuning work of the adaptive rate is unavoidable. In [23], a new method is proposed that combines the finite set model predictive control with an extended Kalman filter (EKF) for online parameter estimation. The proposed method shows robustness to parameter uncertainty and measurement noise; however, the calculation burden of the method is large.

Although there are many papers that study the online inductance estimation in the control of three-phase PWM rectifiers, many inductance estimation methods are conducted under balanced network conditions. Many control methods with inductance estimation that operate under unbalanced network conditions do not take distorted network conditions into consideration. Moreover, the control of the dc-bus voltage of three-phase PWM rectifiers under unbalanced and distorted network conditions is not considered in most of these methods.

This paper proposes a robust DPC method under unbalanced and distorted conditions with online inductance identification. By analyzing the instantaneous power in the input line inductance, a very simple power compensation technique is proposed and added to the original power reference. The reference voltage vector is calculated based on the deadbeat control of the extended power on the grid side and then synthesized by space vector modulation (SVM) [6]. The robustness of the proposed DPC method is improved by introducing online inductance identification based on the proposed gradient correction method. Not only the harmonics in the grid-side currents but also the ripple in the dc-bus voltage are significantly reduced, even with an inaccurate inductance value. The effectiveness of the proposed method is confirmed by the presented simulation and experimental results.

II. Dynamic Equations of a Three-Phase PWM Rectifier

A. Model of a Three-Phase PWM Rectifier Under an Unbalanced Network

Fig. 1 shows the circuit of a three-phase, two-level PWM rectifier, which is connected to the three-phase supply through

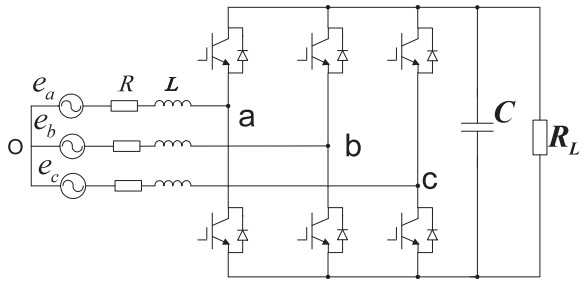

Fig. 1. Topology of a two-level PWM rectifier.

the input line inductance. The model of the three-phase PWM rectifier in the stationary reference frame can be expressed using a complex vector as [6]

$$\boldsymbol{e}_{\alpha\beta} = R\boldsymbol{i}_{\alpha\beta} + L\frac{\mathrm{d}\boldsymbol{i}_{\alpha\beta}}{\mathrm{d}t} + \boldsymbol{v}_{\alpha\beta} \tag{1}$$

where the subscript "$\alpha\beta$" stands for the stationary reference frame. $\boldsymbol{e}_{\alpha\beta} = e_\alpha + \mathrm{j}e_\beta$ is the grid voltage vector, $\boldsymbol{i}_{\alpha\beta} = i_\alpha + \mathrm{j}i_\beta$ is the grid current vector, $\boldsymbol{v}_{\alpha\beta} = v_\alpha + \mathrm{j}v_\beta$ is the rectifier voltage vector, and R and L are the equivalent series resistance and inductance of the input filter, respectively.

According to instantaneous power theory [24], the complex power $\boldsymbol{S}_{in}$ on the grid side can be calculated as

$$\boldsymbol{S}_{in} = P_{in} + jQ_{in} = \frac{3}{2}\left(\boldsymbol{i}^*_{\alpha\beta}\boldsymbol{e}_{\alpha\beta}\right) \tag{2}$$

where "$*$" denotes the conjugate of a complex vector.

In [25], an extended reactive power is proposed, which is suitable for an unbalanced network

$$Q^{\mathrm{nov}}_{in} = \frac{3}{2}\mathrm{Re}\left(\boldsymbol{i}^*_{\alpha\beta}\boldsymbol{e}'_{\alpha\beta}\right) \tag{3}$$

where the variable $\boldsymbol{e}'_{\alpha\beta}$ lags $\boldsymbol{e}_{\alpha\beta}$ by 90 electrical degrees [25].

The model of the three-phase PWM rectifier can be expressed in the synchronous reference frame. All the variables can be transformed from the stationary reference frame to the synchronous reference frame by using the angular frequency of the grid fundamental component ω, and in this paper, $\omega = 2\pi f \approx 314$ rad/s. Under balanced grid conditions, the relationship between the variable in the stationary reference frame $\boldsymbol{x}_{\alpha\beta}$ and the variable in the synchronous reference frame $\boldsymbol{x}_{dq}$ can be expressed as

$$\boldsymbol{x}_{dq} = \boldsymbol{x}_{\alpha\beta} \cdot e^{-\mathrm{j}\omega t} \tag{4}$$

where the subscript "dq" means that the variable is in the synchronous reference frame. Substituting (1) into (4), the voltage equation in the synchronous reference frame can be expressed as

$$\boldsymbol{e}_{dq} = R\boldsymbol{i}_{dq} + L\frac{\mathrm{d}\boldsymbol{i}_{dq}}{\mathrm{d}t} + \mathrm{j}\omega L\boldsymbol{i}_{dq} + \boldsymbol{v}_{dq} \tag{5}$$

where $\boldsymbol{e}_{dq}$, $\boldsymbol{i}_{dq}$, and $\boldsymbol{v}_{dq}$ are the grid voltage vector, the grid current vector, and the rectifier voltage vector in the synchronous reference frame, respectively.

Under unbalanced network conditions, the grid voltages, the grid currents, and the converter voltage can be expressed as [26]

$$\boldsymbol{e}_{\alpha\beta} = \boldsymbol{e}^+_{\alpha\beta} + \boldsymbol{e}^-_{\alpha\beta} = \boldsymbol{e}^+_{dq}e^{j\omega t} + \boldsymbol{e}^-_{dq}e^{-j\omega t} \tag{6}$$

$$\boldsymbol{i}_{\alpha\beta} = \boldsymbol{i}^{+}_{\alpha\beta} + \boldsymbol{i}^{-}_{\alpha\beta} = \boldsymbol{i}^{+}_{dq} e^{j\omega t} + \boldsymbol{i}^{-}_{dq} e^{-j\omega t} \tag{7}$$

$$\boldsymbol{v}_{\alpha\beta} = \boldsymbol{v}^{+}_{\alpha\beta} + \boldsymbol{v}^{-}_{\alpha\beta} = \boldsymbol{v}^{+}_{dq} e^{j\omega t} + \boldsymbol{v}^{-}_{dq} e^{-j\omega t} \tag{8}$$

$$\begin{aligned}\boldsymbol{e}'_{\alpha\beta} &= \boldsymbol{e}^{+}_{dq} e^{j(\omega t - \frac{\pi}{2})} + \boldsymbol{e}^{-}_{dq} e^{-j(\omega t - \frac{\pi}{2})} \\ &= -j\boldsymbol{e}^{+}_{dq} e^{j\omega t} + j\boldsymbol{e}^{-}_{dq} e^{-j\omega t}\end{aligned} \tag{9}$$

$$\begin{aligned}\boldsymbol{i}'_{\alpha\beta} &= \boldsymbol{i}^{+}_{dq} e^{j(\omega t - \frac{\pi}{2})} + \boldsymbol{i}^{-}_{dq} e^{-j(\omega t - \frac{\pi}{2})} \\ &= -j\boldsymbol{i}^{+}_{dq} e^{j\omega t} + j\boldsymbol{i}^{-}_{dq} e^{-j\omega t}\end{aligned} \tag{10}$$

$$\begin{aligned}\boldsymbol{v}'_{\alpha\beta} &= \boldsymbol{v}^{+}_{dq} e^{j(\omega t - \frac{\pi}{2})} + \boldsymbol{v}^{-}_{dq} e^{-j(\omega t - \frac{\pi}{2})} \\ &= -j\boldsymbol{v}^{+}_{dq} e^{j\omega t} + j\boldsymbol{v}^{-}_{dq} e^{-j\omega t}\end{aligned} \tag{11}$$

where $\boldsymbol{e}^{+}_{\alpha\beta} = e^{+}_{\alpha} + je^{+}_{\beta}$, $\boldsymbol{e}^{-}_{\alpha\beta} = e^{-}_{\alpha} + je^{-}_{\beta}$, $\boldsymbol{i}^{+}_{\alpha\beta} = i^{+}_{\alpha} + ji^{+}_{\beta}$, $\boldsymbol{i}^{-}_{\alpha\beta} = i^{-}_{\alpha} + ji^{-}_{\beta}$, $\boldsymbol{v}^{+}_{\alpha\beta} = v^{+}_{\alpha} + jv^{+}_{\beta}$, $\boldsymbol{v}^{-}_{\alpha\beta} = v^{-}_{\alpha} + jv^{-}_{\beta}$, $\boldsymbol{e}^{+}_{dq} = e^{+}_{d} + je^{+}_{q}$, $\boldsymbol{e}^{-}_{dq} = e^{-}_{d} + je^{-}_{q}$, $\boldsymbol{i}^{+}_{dq} = i^{+}_{d} + ji^{+}_{q}$, $\boldsymbol{i}^{-}_{dq} = i^{-}_{d} + ji^{-}_{q}$, $\boldsymbol{v}^{+}_{dq} = v^{+}_{d} + jv^{+}_{q}$, and $\boldsymbol{v}^{-}_{dq} = v^{-}_{d} + jv^{-}_{q}$. The superscript "+" means the positive sequence component (PSC) of the variables, while the superscript "−" denotes the negative sequence component (NSC) of the variables. The delayed grid current $\boldsymbol{i}'_{\alpha\beta}$ lags $\boldsymbol{i}_{\alpha\beta}$ by 90 electrical degrees, and the delayed grid current $\boldsymbol{v}'_{\alpha\beta}$ lags $\boldsymbol{v}_{\alpha\beta}$ by 90 electrical degrees.

From (9)–(11), the PSC and NSC of $\boldsymbol{e}_{\alpha\beta}$, $\boldsymbol{i}_{\alpha\beta}$, and $\boldsymbol{v}_{\alpha\beta}$ can be obtained as

$$\begin{bmatrix}\boldsymbol{e}^{+}_{dq} \\ \boldsymbol{e}^{-}_{dq}\end{bmatrix} = \frac{1}{2}\begin{bmatrix}e^{-j\omega t} & je^{-j\omega t} \\ e^{j\omega t} & -je^{j\omega t}\end{bmatrix}\begin{bmatrix}\boldsymbol{e}_{\alpha\beta} \\ \boldsymbol{e}'_{\alpha\beta}\end{bmatrix} \tag{12}$$

$$\begin{bmatrix}\boldsymbol{i}^{+}_{dq} \\ \boldsymbol{i}^{-}_{dq}\end{bmatrix} = \frac{1}{2}\begin{bmatrix}e^{-j\omega t} & je^{-j\omega t} \\ e^{j\omega t} & -je^{j\omega t}\end{bmatrix}\begin{bmatrix}\boldsymbol{i}_{\alpha\beta} \\ \boldsymbol{i}'_{\alpha\beta}\end{bmatrix} \tag{13}$$

$$\begin{bmatrix}\boldsymbol{v}^{+}_{dq} \\ \boldsymbol{v}^{-}_{dq}\end{bmatrix} = \frac{1}{2}\begin{bmatrix}e^{-j\omega t} & je^{-j\omega t} \\ e^{j\omega t} & -je^{j\omega t}\end{bmatrix}\begin{bmatrix}\boldsymbol{v}_{\alpha\beta} \\ \boldsymbol{v}'_{\alpha\beta}\end{bmatrix}. \tag{14}$$

Under unbalanced network conditions, the active power and extended reactive power on the grid side can be rearranged as the sum of the dc component (denoted as $\bar{X}$) and ac component (denoted as $\tilde{X}$) [6], [17], [27]. These dc and ac components can easily be expressed by using the original grid voltage $\boldsymbol{e}$, the delayed grid voltage $\boldsymbol{e}'$, the original grid current $\boldsymbol{i}$, and the delayed grid current $\boldsymbol{i}'$, that is,

$$P_{in} = \bar{P}_{in} + \tilde{P}_{in} \tag{15}$$

$$Q^{\text{nov}}_{in} = \bar{Q}^{\text{nov}}_{in} + \tilde{Q}^{\text{nov}}_{in} \tag{16}$$

where

$$\bar{P}_{in} = \frac{3}{4}\left(\boldsymbol{i} \odot \boldsymbol{e} + \boldsymbol{i}' \odot \boldsymbol{e}'\right) \tag{17}$$

$$\tilde{P}_{in} = \frac{3}{4}\left(\boldsymbol{i} \odot \boldsymbol{e} - \boldsymbol{i}' \odot \boldsymbol{e}'\right) \tag{18}$$

$$\bar{Q}^{\text{nov}}_{in} = \frac{3}{4}\left(\boldsymbol{i} \odot \boldsymbol{e}' - \boldsymbol{i}' \odot \boldsymbol{e}\right) \tag{19}$$

$$\tilde{Q}^{\text{nov}}_{in} = \frac{3}{4}\left(\boldsymbol{i} \odot \boldsymbol{e}' + \boldsymbol{i}' \odot \boldsymbol{e}\right) \tag{20}$$

where $\boldsymbol{i}$, $\boldsymbol{i}'$, $\boldsymbol{e}$, and $\boldsymbol{e}'$ are under the stationary reference frame.

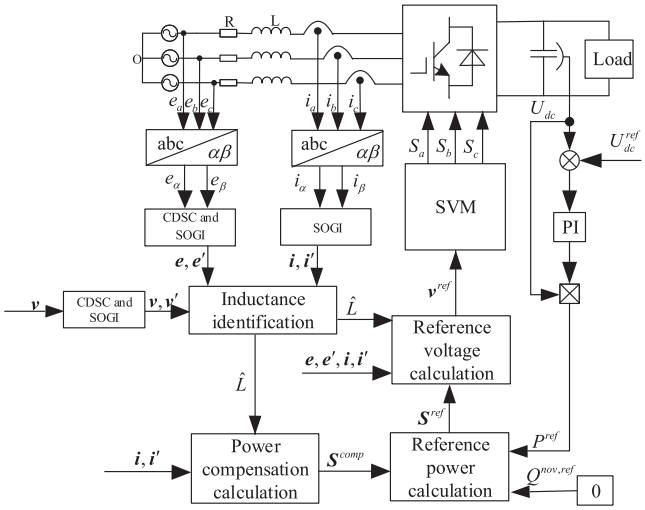

Fig. 2. Control diagram of the proposed robust DPC method under unbalanced and distorted grid voltage conditions.

B. Extension to an Unbalanced and Distorted Network

When the network conditions become unbalanced and distorted, a large number of harmonics are contained in the grid voltage. If these harmonics are not considered in the control methods, then the grid currents will be distorted, and substantial ripple will be present in the dc link voltage. In this paper, a type of cascaded delayed signal cancellation (CDSC) [28] is used to eliminate the low-order harmonics, such as the fifth- and seventh-order harmonic components. Then, the PSC and NSC of the variables can be obtained. A second-order generalized integrator (SOGI) [29] is used to obtain the original variables and the delayed variables. Subsequently, the model of the three-phase PWM rectifier under the unbalanced grid condition is also suitable for unbalanced and distorted network conditions.

III. Principle of DPC Without DC-Bus Voltage Oscillations

A. Reference Power Calculation

Fig. 2 illustrates the overall control diagram of the proposed method. Under unbalanced grid conditions, the derivative of the grid current and its delayed value can be expressed as [6]

$$\frac{\mathrm{d}\boldsymbol{i}}{\mathrm{d}t} = -\omega \cdot \boldsymbol{i}' \tag{21}$$

$$\frac{\mathrm{d}\boldsymbol{i}'}{\mathrm{d}t} = \omega \cdot \boldsymbol{i}. \tag{22}$$

Accordingly, the input inductance voltage $\boldsymbol{u}_L$ and its delayed value $\boldsymbol{u}'_L$ can be calculated from (21) and (22) as

$$\boldsymbol{u}_L = L\frac{\mathrm{d}\boldsymbol{i}}{\mathrm{d}t} = -\omega L \cdot \boldsymbol{i}' \tag{23}$$

$$\boldsymbol{u}'_L = L\frac{\mathrm{d}\boldsymbol{i}'}{\mathrm{d}t} = \omega L \cdot \boldsymbol{i}. \tag{24}$$

From (18) and (20) and from (23) and (24), the ac component of the inductance power can be obtained as

$$\tilde{P}_L = \frac{3}{4}\left(\boldsymbol{i}\odot\boldsymbol{u}_L - \boldsymbol{i}'\odot\boldsymbol{u}'_L\right) = -\frac{3}{2}\omega L\left(\boldsymbol{i}\odot\boldsymbol{i}'\right) \tag{25}$$

$$\tilde{Q}_L^{\text{nov}} = \frac{3}{4}\left(\boldsymbol{i}\odot\boldsymbol{u}'_L + \boldsymbol{i}'\odot\boldsymbol{u}_L\right) = \frac{3}{4}\omega L\left(|\boldsymbol{i}|^2 - |\boldsymbol{i}'|^2\right). \tag{26}$$

The input power ripple is the sum of the inductance power ripple and output power ripple. Because the output power ripple has to be zero to achieve a constant dc-bus voltage, the input power ripple should be equal to the ripple (ac component) of the inductance power. In other words, the power compensation to be added to the input power reference is

$$\begin{aligned}\boldsymbol{S}^{\text{comp}} &= \tilde{P}_L + j\cdot\tilde{Q}_L^{\text{nov}} \\ &= -\frac{3}{2}\omega L\left(\boldsymbol{i}\odot\boldsymbol{i}'\right) + j\cdot\frac{3}{4}\omega L\left(|\boldsymbol{i}|^2 - |\boldsymbol{i}'|^2\right).\end{aligned} \tag{27}$$

Thus, the new complex power reference is obtained as

$$\boldsymbol{S}_{\text{new}}^{\text{ref}} = \boldsymbol{S}^{\text{ref}} + \boldsymbol{S}^{\text{comp}}. \tag{28}$$

B. Reference Voltage Calculation

The derivatives of the active power and extended reactive power on the grid side can be calculated as

$$\frac{\mathrm{d}P_{in}}{\mathrm{d}t} = \frac{3}{2L}\left[|\boldsymbol{e}|^2 - \text{Re}\left(\boldsymbol{v}^*\boldsymbol{e}\right)\right] - \frac{R}{L}P_{in} - \omega Q_{in}^{\text{nov}} \tag{29}$$

$$\frac{\mathrm{d}Q_{in}^{\text{nov}}}{\mathrm{d}t} = \frac{3}{2L}\text{Re}\left[\left(\boldsymbol{e}^* - \boldsymbol{v}^*\right)\boldsymbol{e}'\right] - \frac{R}{L}Q_{in}^{\text{nov}} + \omega P_{in}. \tag{30}$$

Based on the principle of deadbeat power control ($\boldsymbol{S}_{\text{new}}^{\text{ref}} = \boldsymbol{S}^{k+1}$), the equations in (29) and (30) can be discretized by using the first-order Euler method as

$$\begin{aligned}\frac{1}{T_s}\begin{bmatrix} P_{\text{new}}^{\text{ref}} - P_{in}^k \\ Q_{\text{new}}^{\text{ref}} - Q_{in}^{\text{nov},k}\end{bmatrix} &= \frac{3}{2L}\begin{bmatrix} e_\alpha^k e_\alpha^k + e_\beta^k e_\beta^k \\ e_\alpha^k e_\alpha'^k + e_\beta^k e_\beta'^k\end{bmatrix} \\ &\quad - \frac{3}{2L}\begin{bmatrix} e_\alpha^k & e_\beta^k \\ e_\alpha'^k & e_\beta'^k\end{bmatrix}\begin{bmatrix} v_\alpha^k \\ v_\beta^k\end{bmatrix} \\ &\quad - \begin{bmatrix} \frac{R}{L} & \omega \\ -\omega & \frac{R}{L}\end{bmatrix}\begin{bmatrix} P_{in}^k \\ Q_{in}^{\text{nov},k}\end{bmatrix}\end{aligned} \tag{31}$$

where T_s is the control period.

Solving (31), the final reference voltage vector is calculated and expressed using a complex vector as [6]

$$\begin{aligned}\boldsymbol{v}^{\text{ref}} &= \boldsymbol{e}^k - R\boldsymbol{i}^k + j\frac{2\omega L}{3\Delta}\left(Q_{in}^{\text{nov},k}\boldsymbol{e}'^k + P_{in}^k\boldsymbol{e}^k\right) \\ &\quad - j\frac{2L}{3T_s\Delta}\left(\boldsymbol{e}^k\left(Q_{\text{new}}^{\text{ref}} - Q_{in}^{\text{nov},k}\right)\right. \\ &\quad \left. - \boldsymbol{e}'^k\left(P_{\text{new}}^{\text{ref}} - P_{in}^k\right)\right)\end{aligned} \tag{32}$$

where $\Delta = \boldsymbol{e}^k \otimes \boldsymbol{e}'^k = \text{Im}(\boldsymbol{e}^{k*}\boldsymbol{e}'^k)$.

IV. Inductance Identification Based on Gradient Correction Method

A. Basic Principles

Assume that the output of system $y(t)$ can be expressed by the input of the system $h\,(t)$ and the parameter of the system θ. The output of the system is

$$y(t) = \boldsymbol{h}^T(t)\boldsymbol{\theta} \tag{33}$$

where

$$\begin{cases}\boldsymbol{h}(t) = [h_1(t), h_2(t), \ldots, h_N(t)]^T \\ \boldsymbol{\theta} = [\theta_1, \theta_2 \cdots, \theta_N]^T.\end{cases} \tag{34}$$

After discretizing (34), it can be expressed in the standard form for the gradient correction method as

$$y(k) = h^T(k)\theta \tag{35}$$

$$\begin{cases}\boldsymbol{h}(k) = [h_1(k), h_2(k), \ldots, h_N(k)]^T \\ \boldsymbol{\theta} = [\theta_1, \theta_2 \cdots, \theta_N]^T.\end{cases} \tag{36}$$

The basic principle of the gradient correction method is to update the value of the system parameter online by minimizing the following objective function:

$$J(\theta)|_{\hat{\theta}(k)} = \frac{1}{2}\varepsilon^2(\theta, k)|_{\hat{\theta}(k)} \tag{37}$$

where

$$\varepsilon(\theta, k) = y(k) - h^T(k)\theta(k). \tag{38}$$

This is achieved by choosing the appropriate identification value $\hat{\theta}(k)$ along the negative gradient of $J(\theta)$, which can be expressed in recursive form as

$$\hat{\theta}(k) = \hat{\theta}(k-1) - \frac{1}{W(k)}\cdot\text{grad}[J(\hat{\theta}(k-1))] \tag{39}$$

where $W(k)$ is the weighted matrix and grad $[J(\hat{\theta}(k-1))]$ is the gradient direction of the objective function about θ, which is expressed as

$$\text{grad}[J(\hat{\theta}(k-1))] = -h(k)[y(k) - h^T(k)\hat{\theta}(k-1)]. \tag{40}$$

Solving the problem of parameter estimation can be considered as obtaining the solution when the gradient of the objective function is zero.

In the conventional gradient correction method, the weighted matrix is obtained by the Lyapunov stability theorem, which is expressed as

$$W(k) = h^T(k)\cdot h(k).$$

Therefore, the conventional gradient correction method can be arranged as

$$\hat{\theta}(k) = \hat{\theta}(k-1) + \frac{h(k)}{W(k)}[y(k) - h^T(k)\hat{\theta}(k-1)] \tag{41}$$

$$W(k) = h^T(k)\cdot h(k). \tag{42}$$

By using the stochastic approximation algorithm, a recursive formula for the stochastic gradient correction method can be

obtained. That is,

$$\hat{\theta}(k) = \hat{\theta}(k-1) + \frac{h(k)}{W(k)}[y(k) - h^T(k)\hat{\theta}(k-1)] \quad (43)$$

$$W(k) = W(k-1) + \| h(k) \|^2 . \quad (44)$$

B. Forgetting Factor

According to the forgetting factor least squares algorithms in [30], a forgetting factor λ is introduced into the recursive formula (44). The final recursive gradient correction method is expressed as

$$\hat{\theta}(k) = \hat{\theta}(k-1) + \frac{h(k)}{W(k)}[y(k) - h^T(k)\hat{\theta}(k-1)] \quad (45)$$

$$W(k) = \lambda W(k-1) + \| h(k) \|^2 \quad (46)$$

where λ is the forgetting factor $(0 \le \lambda \le 1)$.

The greater the forgetting factor is, the lower the convergence rate of the parameter estimation is. When $\lambda = 1$, (46) is the same as the stochastic gradient correction method shown in (44). The larger the forgetting factor is, the lower will be the convergence rate of the system that is obtained, while the final parameter estimation error fluctuation is relatively small. On the contrary, the smaller the forgetting factor is, the higher will be the convergence rate of the system that is obtained; however, the final parameter estimation error fluctuation is relatively large. There actually exists a tuning process of the forgetting factor, which is based on the convergence rate and the range of the estimation error.

C. Identification Model Under Unbalanced and Distorted Grid Conditions

When using the proposed stochastic gradient correction method to identify the inductance value, all the variables of the three-phase PWM rectifier should be transformed to a synchronous reference frame for obtaining constant values. Because the inductance value is gradually modified along the negative gradient of the objective function in the proposed inductance identification method, if the variables in the objective function are periodic signals, then the gradient of the objective function will fall into a local optimal value rather than the global optimal value. The estimated inductance value will not approach the real value if the gradient of the objective function falls into a local optimal value.

The model of the three-phase PWM rectifier in the synchronous reference frame is shown in (5), which is transformed into matrix form as

$$\begin{bmatrix} e_d \\ e_q \end{bmatrix} = L \begin{bmatrix} \frac{\mathrm{d}i_d}{\mathrm{d}t} \\ \frac{\mathrm{d}i_q}{\mathrm{d}t} \end{bmatrix} + R \begin{bmatrix} i_d \\ i_q \end{bmatrix} + \omega L \begin{bmatrix} -i_q \\ i_d \end{bmatrix} + \begin{bmatrix} v_d \\ v_q \end{bmatrix}. \quad (47)$$

The voltage and current contain different harmonics when the three-phase PWM rectifier operates under unbalanced and distorted network conditions, which will lead to large fluctuations in the parameter identification results. In this paper, an improved identification model is proposed. Only the PSCs of these variables are used in the identification model. That is,

$$\begin{bmatrix} e_d^+ \\ e_q^+ \end{bmatrix} = L \begin{bmatrix} \frac{\mathrm{d}i_d^+}{\mathrm{d}t} \\ \frac{\mathrm{d}i_q^+}{\mathrm{d}t} \end{bmatrix} + R \begin{bmatrix} i_d^+ \\ i_q^+ \end{bmatrix} + \omega L \begin{bmatrix} -i_q^+ \\ i_d^+ \end{bmatrix} + \begin{bmatrix} v_d^+ \\ v_q^+ \end{bmatrix} \quad (48)$$

where the superscript "+" means the PSCs of these variables.

When the three-phase PWM rectifier is under the steady state, it can be assumed that the derivative of the positive component of the current is zero, that is,

$$\begin{cases} \frac{\mathrm{d}i_d^+}{\mathrm{d}t} = 0 \\ \frac{\mathrm{d}i_q^+}{\mathrm{d}t} = 0. \end{cases} \quad (49)$$

Substituting (49) into (48) and rearranging (48) according to the standard form for the gradient correction method that is expressed in (35) and (36), the identification model can be expressed as

$$\begin{bmatrix} e_d^+(k) - v_d^+(k) \\ e_q^+(k) - v_q^+(k) \end{bmatrix} = \begin{bmatrix} i_d^+(k) & -i_q^+(k) \\ i_q^+(k) & i_d^+(k) \end{bmatrix} \begin{bmatrix} R \\ \omega L \end{bmatrix}. \quad (50)$$

Then, the output variable $y(k)$, the input of the system $h(k)$, and the parameter of the system $\theta(k)$ can be expressed as

$$y(k) = \begin{bmatrix} e_d^+(k) - v_d^+(k) \\ e_q^+(k) - v_q^+(k) \end{bmatrix}, \boldsymbol{h}(k) = \begin{bmatrix} i_d^+(k) & -i_q^+(k) \\ i_q^+(k) & i_d^+(k) \end{bmatrix}$$

$$\boldsymbol{\theta} = \begin{bmatrix} R \\ \omega L \end{bmatrix}. \quad (51)$$

Substituting (51) into (37) and (38), the objective function in the proposed control system can be expressed as

$$J(\theta) = \frac{1}{2} \begin{Bmatrix} \left[e_d^+(k) - v_d^+(k) - \left(\hat{R} \cdot i_d^+(k) + \omega \hat{L} \cdot i_q^+(k) \right) \right]^2 \\ \left[e_q^+(k) - v_q^+(k) - \left(-\hat{R} \cdot i_q^+(k) + \omega \hat{L} \cdot i_d^+(k) \right) \right]^2 \end{Bmatrix}. \quad (52)$$

The weighted matrix is a two-dimensional symmetric matrix in the proposed method. The initial weighted matrix is set as a two-dimensional identity matrix, that is,

$$W(0) = \begin{bmatrix} 1 & 0 \\ 0 & 1 \end{bmatrix}. \quad (53)$$

The values in the weighted matrix update in every control period by using (46) in the proposed parameter identification method.

V. Simulation and Experimental Results

To confirm the effectiveness of the proposed method, both simulation and experimental tests are carried out on a two-level

TABLE I
SYSTEM AND CONTROL PARAMETERS

System Parameters	Symbol	Value
Line resistance	R	0.3 Ω
Line inductance	L	10 mH
DC-side capacitor	C	840 μF
Load resistance	R_L	100 Ω
Line-line voltage (RMS)	U_N	150 V
Line voltage frequency	f	50 Hz
DC-side voltage	U_{dc}	300 V
Sampling frequency	f_s	10 kHz

PWM rectifier. The system and control parameters used in the simulation and experimental tests are listed in Table I. In both the simulation tests and the experimental tests, the forgetting factor is selected as 0.999 unless indicated.

A. Simulation Results

The proposed method is simulated in the MATLAB/Simulink environment. The sampling frequency of all the simulation tests is set to 10 kHz. The reference value of the dc-bus voltage is set to 300 V. The grid-side extended reactive power reference value is 0 Var.

To demonstrate that the convergence speed of the stochastic gradient correction method with the forgetting factor is faster than that of the conventional gradient correction method, Figs. 3 and 4 present the simulation results of the two methods. Fig. 3 shows the simulation results of the conventional gradient correction method under balanced grid conditions. Fig. 3(a) presents the identification results of the inductance value when the initial inductance is 30 mH. At the starting point, the inductance value in the controller is much larger than the actual value. In the conventional gradient correction method, the estimated inductance value will drastically decrease at first and then quickly converge to its real value. The estimated inductance values may reach negative values if there is no limit on the estimated values. To avoid a negative value for the estimated inductance value, the estimated value is limited in a range from 2 to 30 mH. Then, the estimated inductance value converges to its real value after a short time. In Fig. 3(b), the initial inductance value is set to 2 mH. The identification algorithm is enabled at 0.05 s, and the identification value slowly converges to its true value in nearly 0.05 s. After the identification is stable, it can be seen that the identification error is small.

Fig. 4 shows the simulation waveform of the proposed stochastic gradient correction method with the forgetting factor under balanced grid conditions. Similar to Fig. 3, the initial inductance values are set to 30 mH in Fig. 4(a) and 2 mH in Fig. 4(b). After the identification algorithm is enabled, the identification value converges quickly in less than 0.02 s. The identification error is small after the estimated inductance values reach the actual values. This finding shows that the tracking capability of the proposed stochastic gradient correction method is

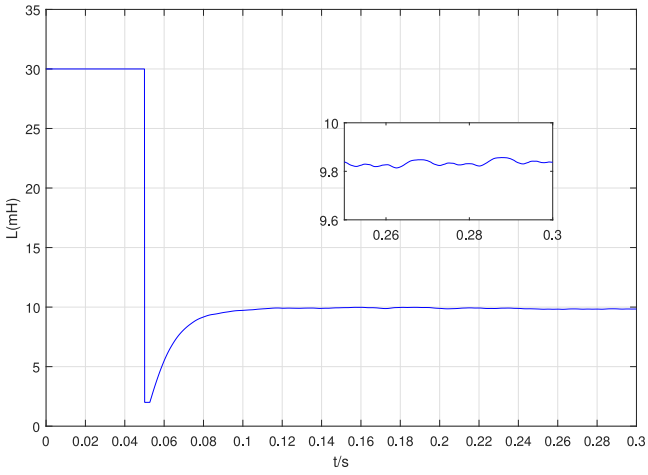

(a)

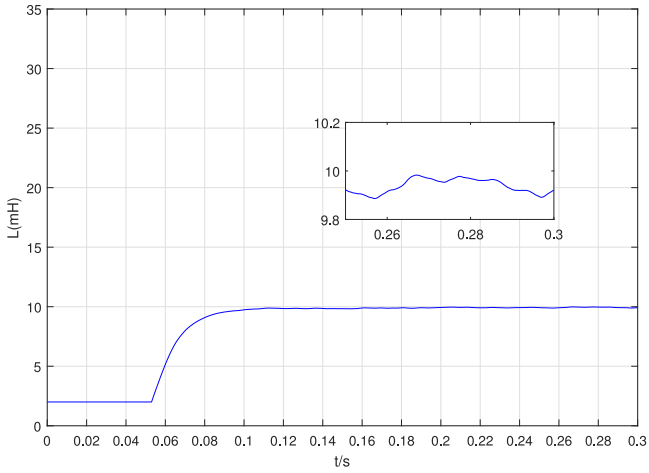

(b)

Fig. 3. Simulated inductance value identification results using the conventional gradient correction method under balanced grid conditions: (a) initial inductance value of 30 mH; (b) initial inductance value of 2 mH.

considerably improved. In Fig. 4(b), the initial inductance value in the controller is set as 2 mH. This differs greatly from the real value of the input-side inductance value, 10 mH. Therefore, some errors are produced in the grid-side currents in the proposed method at first. Then a large error emerges in the estimated inductance value because the grid currents are used in the inductance estimation process. However, the estimated inductance value reaches its real value immediately. In the simulation results in Fig. 8, this overshoot in such a short time has little influence on the control performance. In Fig. 4(b), the final estimated inductance value is around 9.92 mH. The error in the final estimated inductance value is only 1% when compared with the real value. The estimated inductance value is thus very close to the real value of the inductance.

To show the impact of the forgetting factor, two simulation tests are conducted on the control system under unbalanced and distorted network conditions. In the simulation tests, the phase A grid voltage dips to 50% of its initial value, and 10% of the fifth-order harmonic component and 10% of the seventh-order

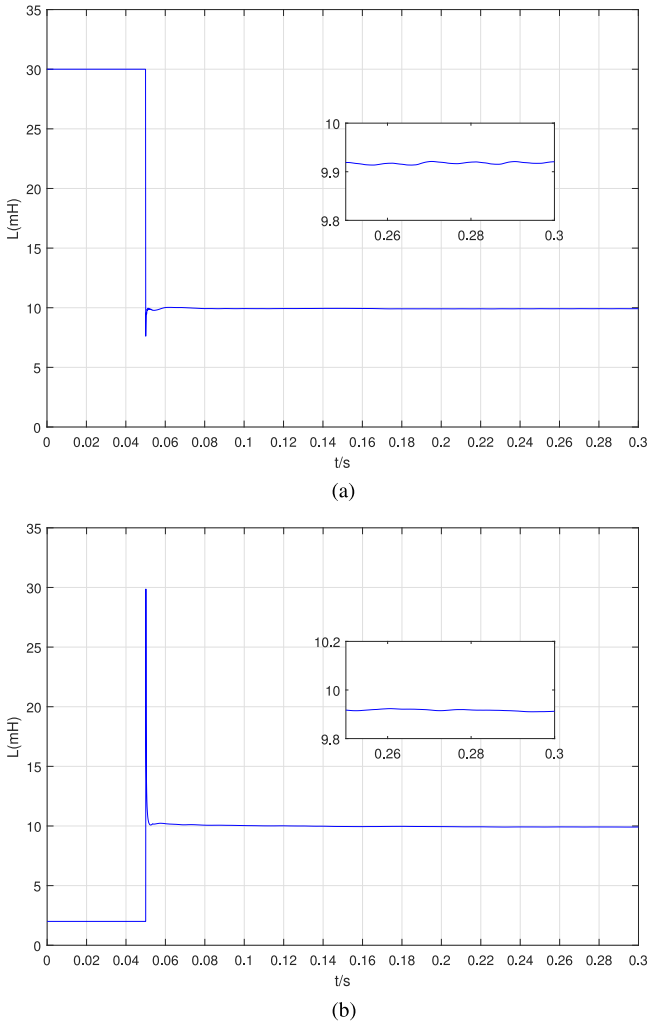

Fig. 4. Inductance value identification results using the stochastic gradient correction method with the forgetting factor under balanced grid conditions: (a) initial inductance value of 30 mH; (b) initial inductance value of 2 mH.

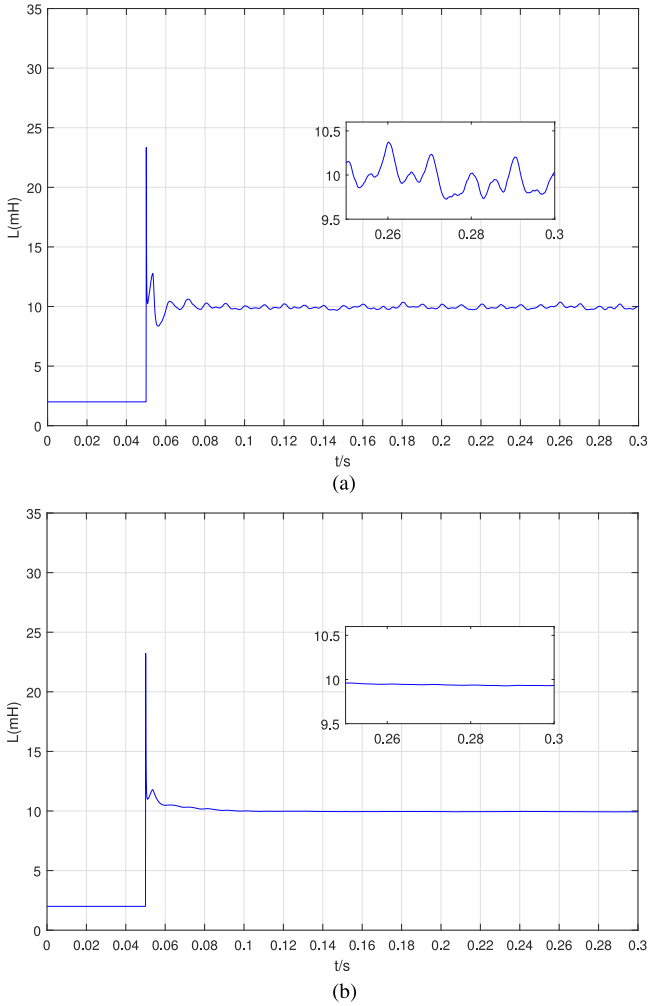

Fig. 5. Inductance identification results using the stochastic gradient correction method with the forgetting factor under unbalanced and distorted network conditions when the initial inductance value is set to 2 mH: (a) the forgetting factor is 0.8; (b) the forgetting factor is 0.999.

harmonic component are added to the grid voltage. In Fig. 5(a), the forgetting factor is set as 0.8. The initial value of the input-side inductance is 2 mH. The convergence rate of the proposed method when the forgetting factor is 0.8 is higher than that of the proposed method when the forgetting factor is 0.999. However, compared with the steady-state estimation errors when the forgetting factor of the proposed method is 0.8, the estimation errors are smaller when the forgetting factor is 0.999.

A DPC method to achieve the control target of eliminating the dc-link voltage oscillations and maintaining the sinusoidal grid currents under unbalanced network conditions is proposed in [27]. The method in [27] is compared with the proposed method in this manuscript under the same simulation conditions. In the simulation tests, the phase A grid voltage first dips to 50% of its initial value. Ten percent of the fifth-order harmonic component and 10% of the seventh-order harmonic component are added to the grid voltages at 0.1 s. The initial inductance value applied in the controller is the actual value of the grid-side inductance, 10 mH. The inductance value in the controller changes at 0.2 s. Figs. 6 and 8 present the simulation results of the two methods; from top to bottom, the curves are the inductance value used in the proposed DPC method, grid-side active power, extended reactive power, dc-bus voltage, grid voltages, and grid-side currents.

The inductance value used in the controller changes from 10 to 30 mH at 0.2 s in Fig. 6(a). The proposed inductance identification method is enabled at 0.3 s, and the inductance value in the controller converges to the actual value immediately. The ripples in the power and the harmonics in the input-side currents are much reduced, and the ripples in the dc-bus voltage are eliminated after 0.3 s. However, in Fig. 6(b), some low-order harmonics emerge in the input-side currents when the grid voltages become unbalanced and distorted even with the real inductance value because distorted network conditions are not considered in [27]. Without the parameter identification method proposed in this manuscript, substantial harmonics are produced in the grid-side power and current in the method of [27] after the inductance value in the controller becomes 30 mH (300% of actual value).

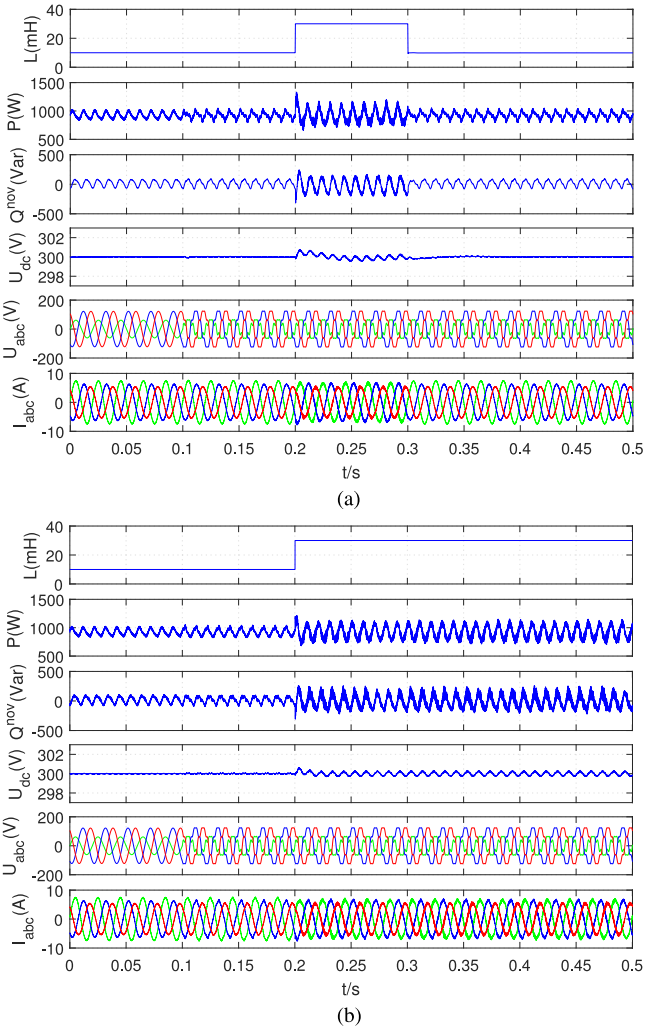

Fig. 6. Simulation results of two DPC methods when the inductance value in the controller changes to 30 mH: (a) proposed DPC method with the proposed online inductance identification method enabled at $t = 0.3$ s; (b) DPC method in [27].

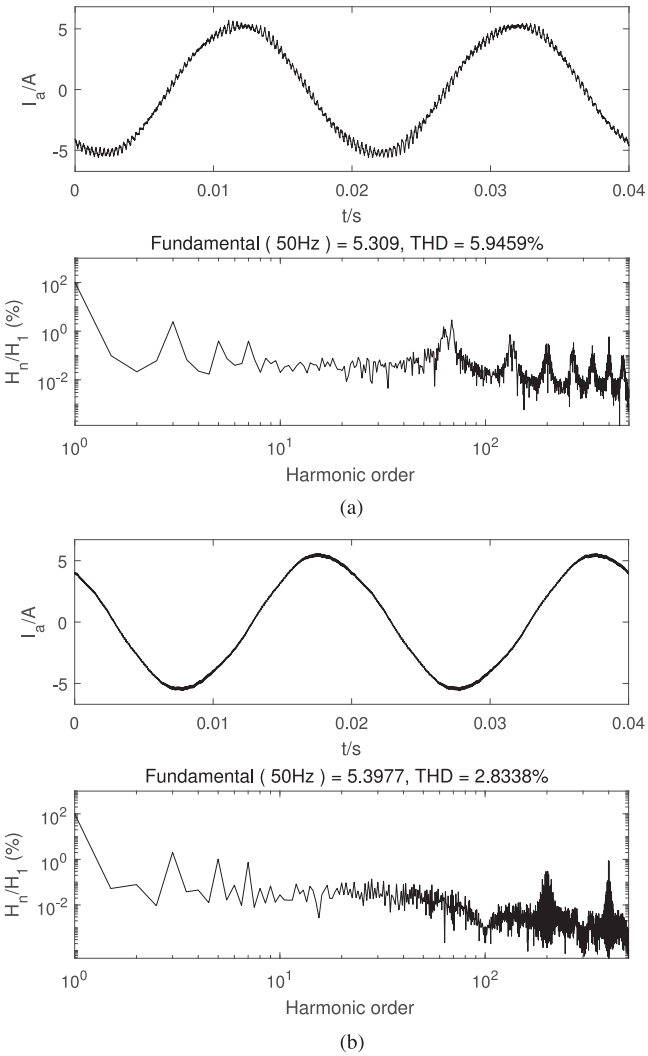

Fig. 7. Harmonic spectrum of the grid current of the proposed method before and after enabling the online inductance identification: (a) before enabling the online identification with an initial inductance value of 30 mH; (b) after enabling the online identification.

The ripples in the dc-bus voltage remain all the time in Fig. 6(b) after the grid voltages become unbalanced and distorted.

Fig. 7 presents the total harmonic distortion (THD) of the phase A grid current of the DPC method proposed in this paper before and after enabling the parameter identification method. The THD of the phase A grid current is 5.95% when the inductance value in the controller is 30 mH. The THD is decreased to 2.83% after the proposed inductance identification method is enabled.

In Fig. 8, the grid voltages change from unbalanced to unbalanced and distorted at 0.1s. Before 0.2 s, the inductance value in the controller is the same as the actual inductance value, 10 mH. The inductance value in the controller of the two methods changes to 2 mH at 0.2 s. The main control algorithm of the proposed method is DPC with SVM. The voltage reference value is directly calculated by the mathematical model and parameter of the three-phase PWM rectifier. If the inductance value in the controller deviates too much from the real value of the inductance, undesirable grid-side currents will be produced. The grid-side extended reactive power is calculated by using grid voltages and grid currents. The currents obtained by the mismatched inductance value have impacts on the steady-state errors of the grid-side extended power. In Fig. 8(a), there is an undesirable dc offset in the grid-side extended reactive power when the inductance value in the controller is 2 mH. After the inductance identification method is enabled, the dc offset in the extended reactive power is eliminated, and the ripples in the dc-bus voltage are much reduced. Because distorted network conditions are not considered in [27], some obvious low-order harmonics are shown in the grid-side currents in Fig. 8(b) under unbalanced and distorted network conditions with matched or mismatched inductance values. Also, some ripples emerge after the inductance value in the controller changes to 2 mH.

From the simulation results above, it may be observed that the previous method proposed in [27] is not robust to changes in the inductance value, and its control performance is downgraded under unbalanced and distorted network conditions.

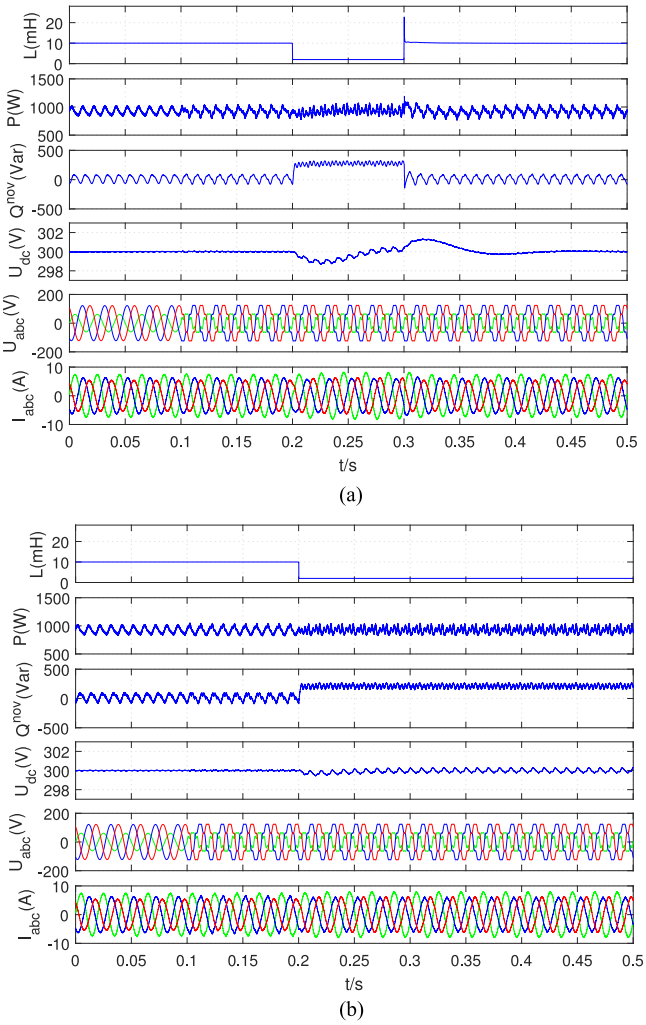

Fig. 8. Simulation results of two DPC methods when the inductance value in the controller changes to 2 mH: (a) proposed DPC method with the proposed online inductance identification method enabled at $t = 0.3$ s; (b) DPC method in [27].

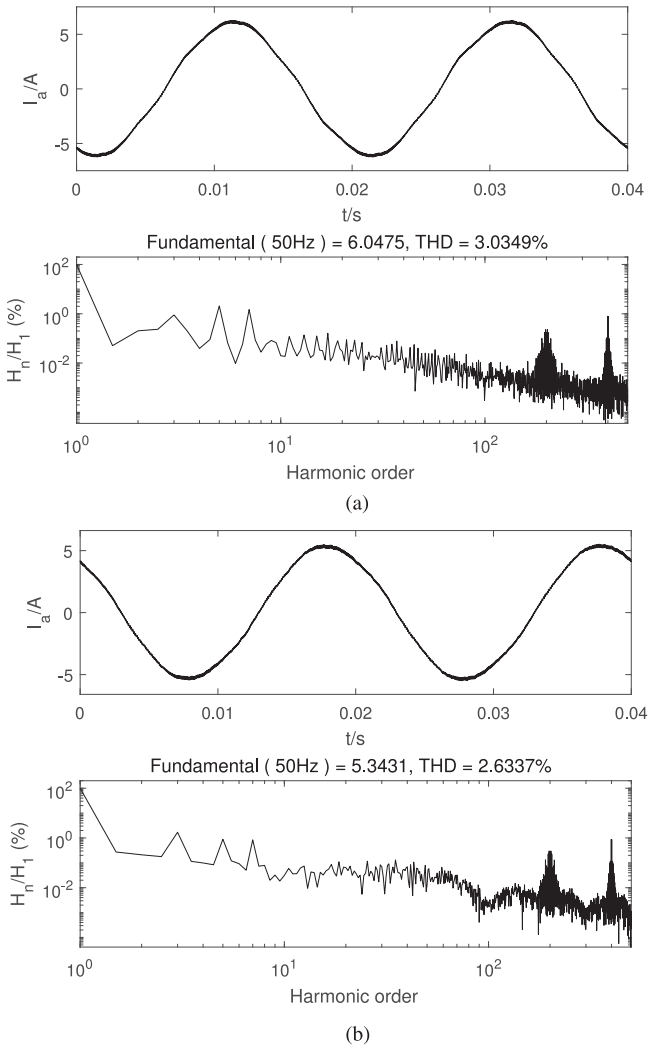

Fig. 9. Harmonic spectrum of the grid current of the proposed method before and after enabling the online inductance identification: (a) before enabling the online identification with an initial inductance value of 2 mH; (b) after enabling the online identification.

However, the method proposed in this paper achieves better control performance under unbalanced and distorted network conditions. The proposed method is robust to changes in the inductance value because the inductance identification method is applied in the DPC method.

Fig. 9 shows the harmonic spectra of the phase A grid current in the proposed method before and after enabling the online inductance identification. When the inductance value is 2 mH, the THD of the phase A grid current is 3.03%. After enabling the inductance identification, the THD is decreased to 2.63%.

In Fig. 10, the real values of the grid-side inductance and the inductance value in the controller are the same at first, that is, 10 mH. The real value of the inductance changes to 5 mH at 0.1 s. Substantial harmonics are then produced in the grid-side power and current, and some ripples emerge in the dc-link voltage. The proposed inductance identification method is enabled at 0.2 s. After that, the estimated inductance value used in the controller immediately converges to nearly 5 mH. The proposed DPC method achieves satisfactory performance again because

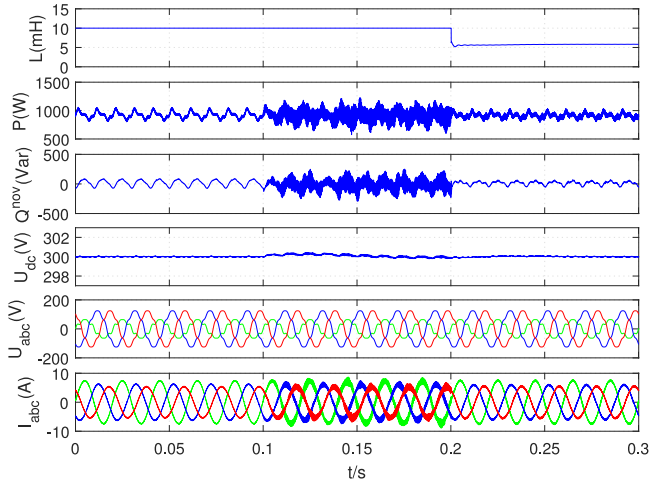

Fig. 10. Simulation results of the proposed DPC under unbalanced and distorted grid network conditions when the real input-side inductance value changes from 10 to 5 mH at $t = 0.1$ s and the online inductance identification method is enabled at $t = 0.2$ s.

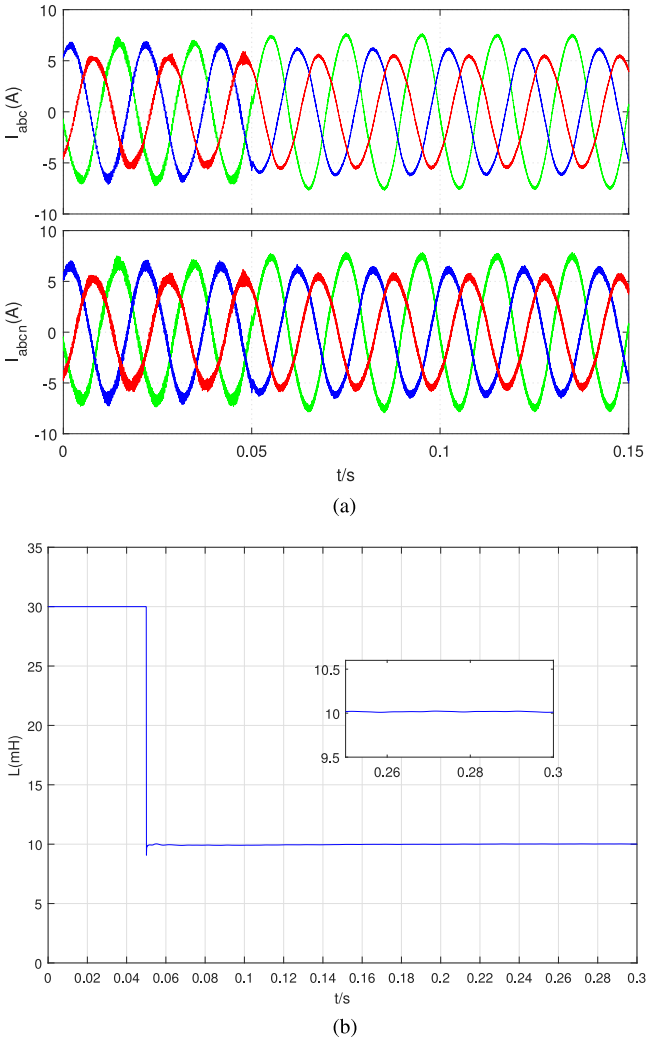

Fig. 11. Simulation results of the inductance value identification method with grid currents with measurement noise under unbalanced and distorted network conditions: (a) original measured grid-side currents I_{abc} and grid-side currents with measurement noise I_{abcn}; (b) inductance identification result when the initial inductance value is 30 mH (300% of actual inductance value).

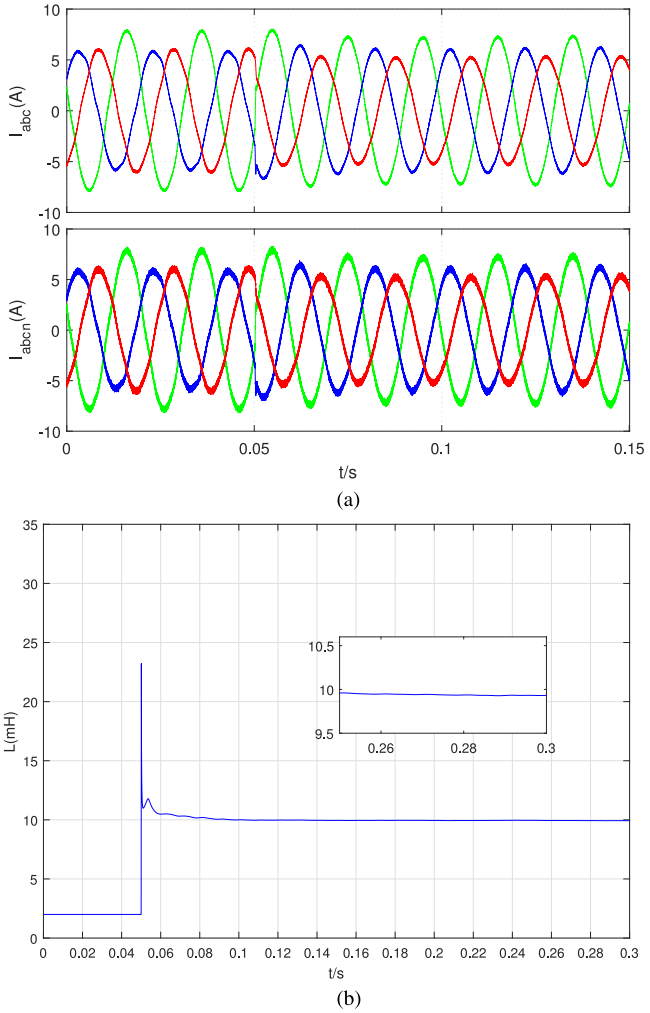

Fig. 12. Simulation results of the inductance value identification method with grid currents with measurement noise under unbalanced and distorted network conditions: (a) original measured grid-side currents I_{abc} and grid-side currents with measurement noise I_{abcn}; (b) inductance identification result when the initial inductance value is 2 mH (20% of actual inductance value).

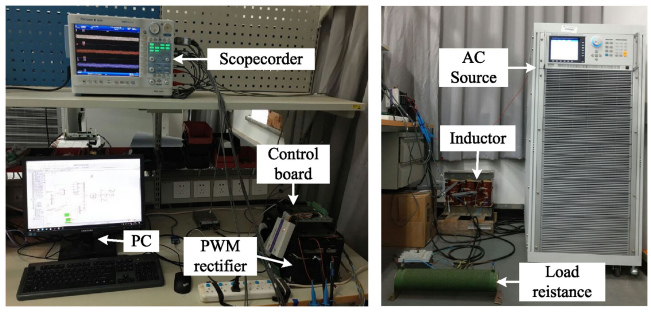

Fig. 13. Experimental test setup: (a) main circuit, control circuit, and oscilloscope; (b) line inductor, programmable ac source, and load.

the real inductance value and the estimated values are matched. This case helps to illustrate that once the forgetting factor is confirmed, the convergence rate remains fast when the real grid-side inductance value and the grid change. A satisfactory identification result is obtained by using the same forgetting factor as before, which is 0.999. The simulation results presented here confirm that a similar quick convergence rate can be achieved by one selected forgetting factor when sudden changes happen in the applied inductance value in the controller or in the real inductance value.

In experimental tests, outer electromagnetic interference may influence the measurement instrument on the experimental rigs, causing measurement noise to emerge. The performance of the parameter identification methods may be downgraded by the measurement noise. However, the proposed inductance identification is robust to the current measurement noise. In the simulation results in Figs. 11 and 12, a white noise is added to the measured grid-side currents. The amplitude of the white noise added to the currents is around 0.4 A. The noise generated in the AD block in the real experimental rig is simulated. In Fig. 11(a), the first channel shows the original measured grid-side current I_{abc}, and the second channel is the current with measurement noise I_{abcn}. In Fig. 11(b), the initial inductance value is set to

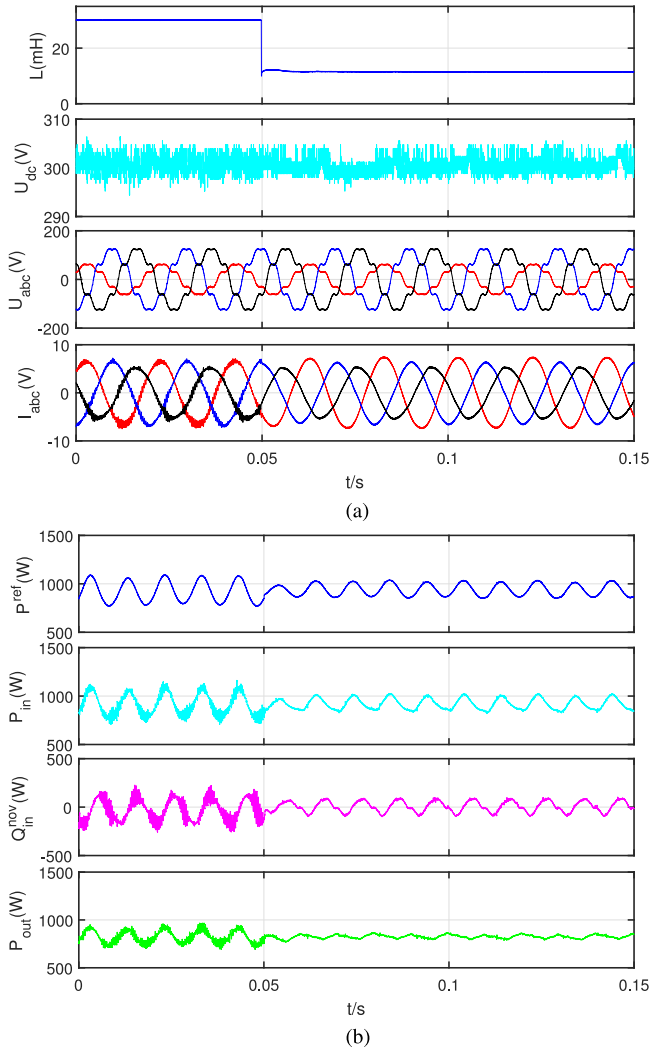

Fig. 14. Experimental results of the proposed DPC under unbalanced and distorted network conditions when enabling the online inductance identification at $t = 0.05$ s with an initial inductance value of 30 mH (300% of actual value).

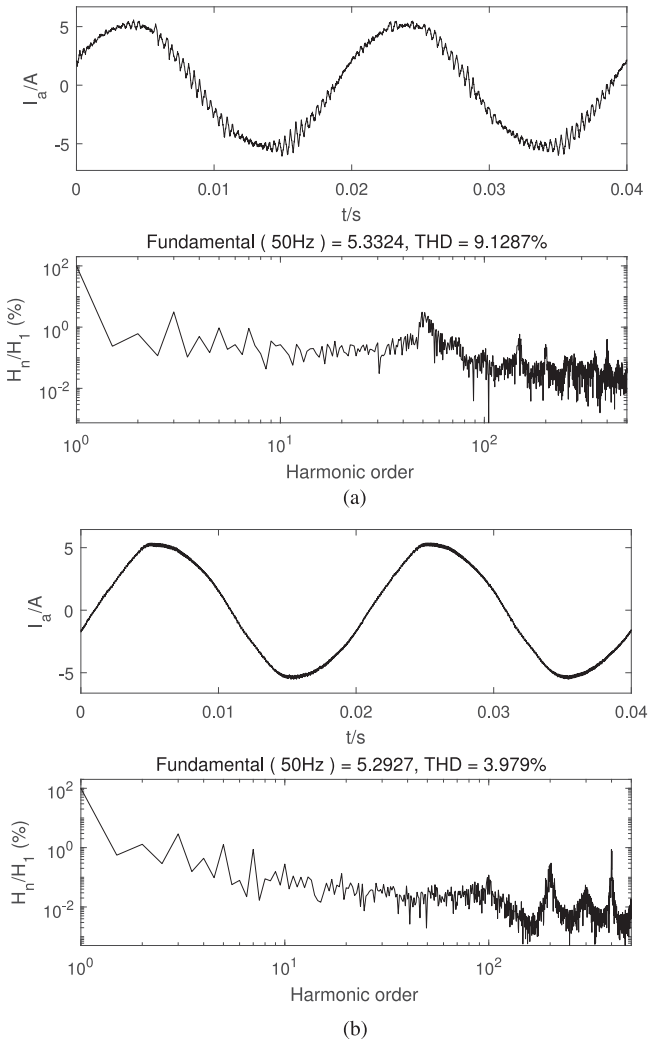

Fig. 15. Harmonic spectrum of grid current in the experiment before and after enabling the online inductance identification: (a) before enabling the online identification with an initial inductance value of 30 mH; (b) after enabling the online identification.

30 mH, and the proposed parameter identification method is enabled at 0.05 s. The estimated inductance value quickly converges to the real value of the inductance without the influence of the measurement noise in the current. The initial inductance value is set as 2 mH in Fig. 12. When the proposed method is enabled at 0.05 s, the inductance value converges to its real value immediately without the influence of measurement noise. The simulation result shows that the proposed method is robust to the measurement noise; even when measurement noise is present, the final parameter identification result will still be satisfactory.

B. Experimental Results

To further validate the effectiveness of the proposed method, the proposed DPC method with inductance identification is tested on a two-level, three-phase PWM rectifier, and the experimental setup is illustrated in Fig. 13. All the tests are performed under unbalanced and distorted grid conditions. The 32-bit floating DSP TMS320F28335 is used to implement the control algorithm. In all the tests, the reference value of the input-side active power P_{in}^{ref}, real value of the input-side active power P_{in}, input-side extended reactive power Q_{in}^{nov}, output-side active power P_{out}, and estimated inductance $\hat{L}$ are displayed and recorded by a digital oscilloscope via a DA converter. The dc-bus voltage, grid voltages, and grid currents are directly measured by voltage/current probes connected to a DL850 scope coder. A programmable ac source (Chroma 61511) is used to generate the required distorted grid conditions. In the experimental tests, the phase A grid voltage dips to 50% of its initial value, 43.5 V, and 10% of the fifth-order harmonic component and 10% of the seventh-order harmonic component are added to the grid voltage. All the experimental tests are conducted under voltage closed-loop control. The reference value of the dc-link bus voltage is set to 300 V, and the grid-side extended reactive power reference value is 0 Var.

Fig. 14 shows the experimental results of the proposed DPC method with inductance identification. The initial inductance value is 30 mH in Fig. 14. When the inductance value used in the

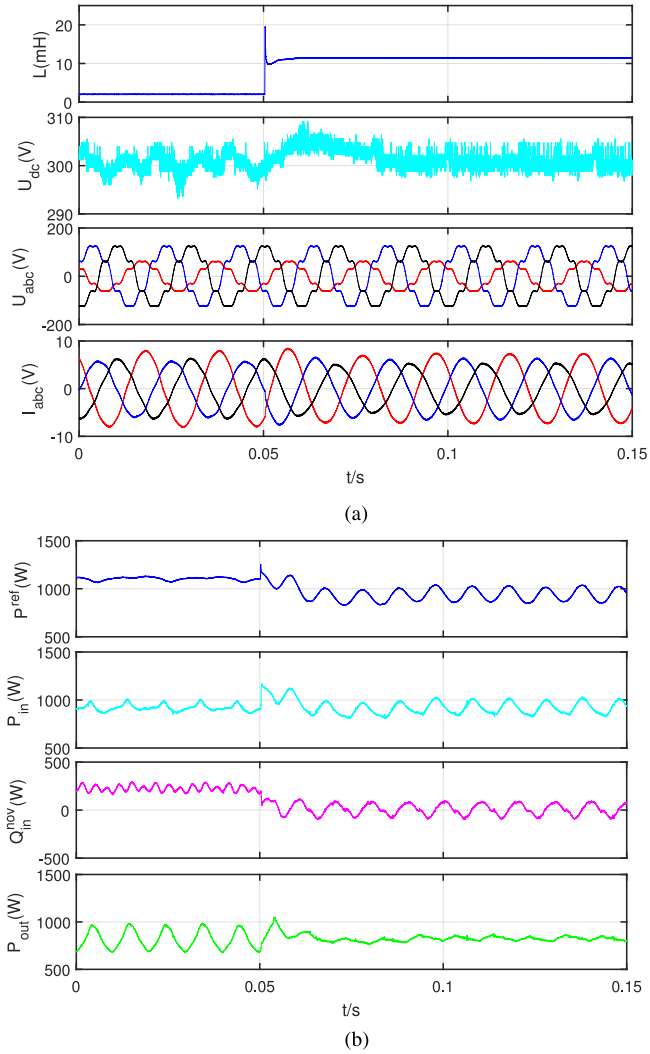

Fig. 16. Experimental results of the proposed DPC under unbalanced and distorted network conditions when enabling the online inductance identification at $t = 0.05$ s with an initial inductance value of 2 mH (20% of actual value).

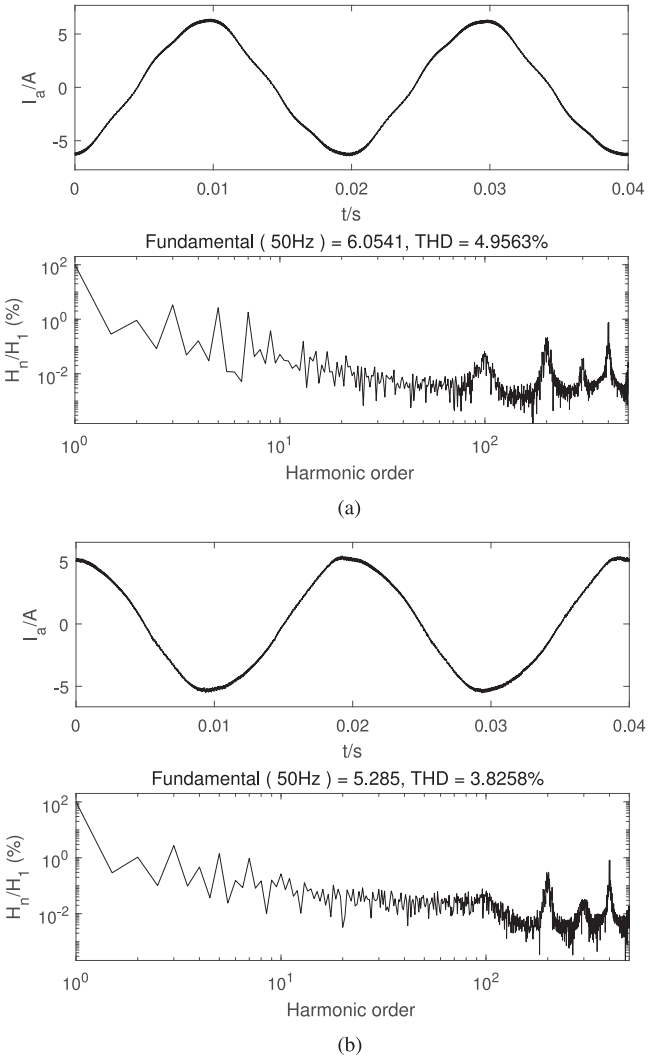

Fig. 17. Harmonic spectrum of grid current in experiment before and after enabling the online inductance identification: (a) before enabling the online identification with an initial inductance value of 2 mH; (b) after enabling the online identification.

control system is 30 mH, the grid-side current contains serious distortion, and the grid-side reference active power, grid-side active power, grid-side extended reactive power, and output-side active power fluctuate drastically. The identification algorithm is enabled at 0.05 s, and the identification value quickly converges to the real inductance value. Then, the fluctuations of the grid-side active power reference value, the grid-side active power, the grid side extended reactive power, and the output-side power are reduced to relatively small ranges.

Fig. 15 is the phase A grid current THD analysis of Fig. 14(a). Before the identification algorithm is enabled, the THD of the phase A current is 9.1287%. A clear current distortion can be observed in the phase A current. After the inductance identification algorithm is enabled, the inductance value is identified by the stochastic gradient correction method with a forgetting factor. The THD of the phase A current decreases to 3.979%. As shown in Fig. 14(a), the three-phase grid current is sinusoidal.

Fig. 16 shows the experimental results of the proposed DPC method when the initial inductance value is 2 mH. The stochastic gradient correction inductance identification with a forgetting factor is utilized in the DPC for improving the performance when the inductance value deviates from its real value. There is an undesirable dc offset in the grid-side extended reactive power when the inductance value used in the control system is 2 mH. The dc component of the extended reactive power is approximately 250 Var. Similar to the simulation result in Fig. 8, the power factor is affected. The grid-side current is slightly distorted, and there are fluctuations in the active power reference value and the actual active power. An observable ripple appears in the output-side active power and dc-bus voltage.

At 0.05 s, the identification algorithm is enabled, the inductance identification value converges rapidly, and the identification value finally remains at 11 mH. During the dynamic identification process, the bus voltage deviates from its reference value in a short time. After the estimated inductance value is stable, the bus voltage firmly remains at the reference value of 300 V

with little fluctuation, and the fluctuation of the converter-side output power decreases accordingly. Fig. 17 is the phase A current THD analysis of the grid-side current in Fig. 16(a). When the inductance is 2 mH, the phase A current THD is 4.9563%. It is observable that the phase A current is slightly distorted. After the estimated inductance value becomes stable, the phase A current THD decreases to 3.8258%.

VI. Conclusion

In this paper, an improved DPC method with online inductance identification for PWM rectifiers is proposed. The proposed DPC method is suitable for unbalanced and distorted grid conditions. Compared to prior DPC methods, the method in this paper not only takes the performance improvement of the input-side power and current into account but also considers eliminating the ripple in the dc-bus voltage and output-side active power. Moreover, it can operate under unbalanced and distorted grid conditions by utilizing the CDSC and SOGI to extract the original voltage and current and their delayed values. The power compensation can be obtained through analyzing the power ripple in the input side, output side, and inductance. The power compensation is added to the original power reference as a new power reference value. The ultimate voltage reference value can be calculated by using the principle of deadbeat power control and finally synthesized by SVM. An online inductance identification technique is introduced to the proposed DPC. This identification method is based on the stochastic gradient correction with a forgetting factor. It can estimate the actual value of the inductance when the inductance value deviates from its real value. The superior performance of the proposed method is validated by simulation and experimental results.

References

[1] J. Rodriguez, J. Dixon, J. Espinoza, J. Pontt, and P. Lezana, "PWM regenerative rectifiers: State of the art," *IEEE Trans. Ind. Electron.*, vol. 52, no. 1, pp. 5–22, Feb. 2005.

[2] F. Blaabjerg, R. Teodorescu, M. Liserre, and A. V. Timbus, "Overview of control and grid synchronization for distributed power generation systems," *IEEE Trans. Ind. Electron.*, vol. 53, no. 5, pp. 1398–1409, Oct. 2006.

[3] J. Alonso-Martinez, J. E. Carrasco, and S. Arnaltes, "Table-based direct power control: A critical review for microgrid applications," *IEEE Trans. Power Electron.*, vol. 25, no. 12, pp. 2949–2961, Dec. 2010.

[4] A. Yazdani and R. Iravani, *Voltage-Sourced Converters in Power Systems*. Hoboken, NJ, USA: Wiley-IEEE Press, 2010.

[5] T. Noguchi, H. Tomiki, S. Kondo, and I. Takahashi, "Direct power control of PWM converter without power-source voltage sensors," *IEEE Trans. Ind. Appl.*, vol. 34, no. 3, pp. 473–479, May/Jun. 1998.

[6] Y. Zhang and C. Qu, "Direct power control of a pulse width modulation rectifier using space vector modulation under unbalanced grid voltages," *IEEE Trans. Power Electron.*, vol. 30, no. 10, pp. 5892–5901, Oct. 2015.

[7] Y. Zhang, J. Gao, and C. Qu, "Relationship between two direct power control methods for PWM rectifiers under unbalanced network," *IEEE Trans. Power Electron.*, vol. 32, no. 5, pp. 4084–4094, May 2017.

[8] Y. Zhang, Z. Li, Y. Zhang, W. Xie, Z. Piao, and C. Hu, "Performance improvement of direct power control of PWM rectifier with simple calculation," *IEEE Trans. Power Electron.*, vol. 28, no. 7, pp. 3428–3437, Jul. 2013.

[9] Y. Zhang, J. Liu, H. Yang, and J. Gao, "Direct power control of pulsewidth modulated rectifiers without dc voltage oscillations under unbalanced grid conditions," *IEEE Trans. Ind. Electron.*, vol. 65, no. 10, pp. 7900–7910, Oct. 2018.

[10] H. Yang, Y. Zhang, J. Liang, J. Gao, P. D. Walker, and N. Zhang, "Sliding-mode observer based voltage-sensorless model predictive power control of PWM rectifier under unbalanced grid conditions," *IEEE Trans. Ind. Electron.*, vol. 65, no. 7, pp. 5550–5560, Jul. 2018.

[11] Y. Zhang, J. Jiao, J. Liu, and J. Gao, "Direct power control of PWM rectifier with feedforward compensation of dc-bus voltage ripple under unbalanced grid conditions," *IEEE Trans. Ind. Appl.*, to be published.

[12] H. Yang, Y. Zhang, J. Liang, J. Liu, N. Zhang, and P. D. Walker, "Robust deadbeat predictive power control with a discrete-time disturbance observer for PWM rectifiers under unbalanced grid conditions," *IEEE Trans. Power Electron.*, vol. 34, no. 1, pp. 287–300, Jan. 2019.

[13] Y. Suh and T. A. Lipo, "Control scheme in hybrid synchronous stationary frame for PWM ac/dc converter under generalized unbalanced operating conditions," *IEEE Trans. Ind. Appl.*, vol. 42, no. 3, pp. 825–835, May 2006.

[14] C. Cheng and H. Nian, "Low-complexity model predictive stator current control of DFIG under harmonic grid voltages," *IEEE Trans. Energy Convers.*, vol. 32, no. 3, pp. 1072–1080, Sep. 2017.

[15] L. Shang, D. Sun, and J. Hu, "Sliding-mode-based direct power control of grid-connected voltage-sourced inverters under unbalanced network conditions," *IET Power Electron.*, vol. 4, no. 5, pp. 570–579, 2011.

[16] J. Eloy-Garcia, S. Arnaltes, and J. Rodriguez-Amenedo, "Direct power control of voltage source inverters with unbalanced grid voltages," *IET Power Electron.*, vol. 1, no. 3, pp. 395–407, 2008.

[17] Z. Li, Y. Li, P. Wang, H. Zhu, C. Liu, and W. Xu, "Control of three-phase boost-type PWM rectifier in stationary frame under unbalanced input voltage," *IEEE Trans. Power Electron.*, vol. 25, no. 10, pp. 2521–2530, Oct. 2010.

[18] Q. N. Trinh, P. Wang, and F. H. Choo, "An improved control strategy of three-phase PWM rectifiers under input voltage distortions and dc-offset measurement errors," *IEEE J. Emerg. Sel. Topics Power Electron.*, vol. 5, no. 3, pp. 1164–1176, Sep. 2017.

[19] X. H. Wu, S. K. Panda, and J. X. Xu, "Design of a plug-in repetitive control scheme for eliminating supply-side current harmonics of three-phase PWM boost rectifiers under generalized supply voltage conditions," *IEEE Trans. Power Electron.*, vol. 25, no. 7, pp. 1800–1810, Jul. 2010.

[20] A. Luo, G. Jin, H. Xiao, Q. Xiong, Y. Wang, and N. Xie, "Simple control method for three-phase pulse-width modulation rectifier of switching power supply under unbalanced and distorted supply voltages," *IET Power Electron.*, vol. 7, no. 10, pp. 2572–2581, 2014.

[21] S. Kwak, U.-C. Moon, and J.-C. Park, "Predictive-control-based direct power control with an adaptive parameter identification technique for improved AFE performance," *IEEE Trans. Power Electron.*, vol. 29, no. 11, pp. 6178–6187, Nov. 2014.

[22] A. Bechouche, D. O. Abdeslam, H. Seddiki, and A. Rahoui, "Estimation of equivalent inductance and resistance for adaptive control of three-phase PWM rectifiers," in *Proc. 42nd Annu. Conf. IEEE Ind. Electron. Soc.*, Oct. 2016, pp. 1336–1341.

[23] M. Abdelrahem, C. M. Hackl, and R. Kennel, "Finite set model predictive control with on-line parameter estimation for active frond-end converters," *Elect. Eng.*, vol. 100, no. 3, pp. 1497–1507, 2018.

[24] H. Akagi, Y. Kanazawa, and A. Nabae, "Instantaneous reactive power compensators comprising switching devices without energy storage components," *IEEE Trans. Ind. Appl.*, vol. IA-20, no. 3, pp. 625–630, May 1984.

[25] Y. Suh and T. A. Lipo, "Modeling and analysis of instantaneous active and reactive power for PWM ac/dc converter under generalized unbalanced network," *IEEE Trans. Power Del.*, vol. 21, no. 3, pp. 1530–1540, Jul. 2006.

[26] H.-S. Song and K. Nam, "Dual current control scheme for PWM converter under unbalanced input voltage conditions," *IEEE Trans. Ind. Electron.*, vol. 46, no. 5, pp. 953–959, Oct. 1999.

[27] Y. Zhang, J. Liu, and J. Gao, "Direct power control of PWM rectifier under unbalanced network using extended power theory," in *Proc. IEEE Energy Convers. Congress Expo.*, Oct. 2017, pp. 4617–4621.

[28] Y. F. Wang and Y. W. Li, "Three-phase cascaded delayed signal cancellation PLL for fast selective harmonic detection," *IEEE Trans. Ind. Electron.*, vol. 60, no. 4, pp. 1452–1463, Apr. 2013.

[29] P. Rodríguez, A. Luna, R. S. Muñoz-Aguilar, I. Etxeberria-Otadui, R. Teodorescu, and F. Blaabjerg, "A stationary reference frame grid synchronization system for three-phase grid-connected power converters under adverse grid conditions," *IEEE Trans. Power Electron.*, vol. 27, no. 1, pp. 99–112, Jan. 2012.

[30] F. Ding and T. Chen, "Performance bounds of forgetting factor least-squares algorithms for time-varying systems with finite measurement data," *IEEE Trans. Circuits Syst. I*, vol. 52, no. 3, pp. 555–566, Mar. 2005.

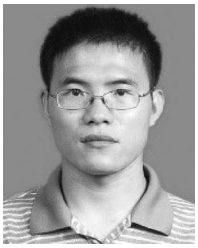

Yongchang Zhang (M'10–SM'18) received the B.S. degree from Chongqing University, Chongqing, China, and the Ph.D. degree from Tsinghua University, Beijing, China, both in electrical engineering, in 2004 and 2009, respectively.

From August 2009 to August 2011, he was a Postdoctoral Fellow with the University of Technology Sydney, Ultimo, Australia. In August 2011, he joined as an Associate Professor with the North China University of Technology, Beijing, China. He is currently a Full Professor and the Director of Inverter Technologies Engineering Research Center of Beijing. He has published more than 100 technical papers in the area of motor drives, pulsewidth modulation, and ac/dc converters. His current research interest is model predictive control for power converters and motor drives.

Prof. Zhang is a Fellow of IET.

Jian Jiao was born in 1993. He received the B.S. degree in electrical engineering from Shijiazhuang Tiedao University, Hebei, China, in 2015. He is currently working toward the M.S. degree in electrical engineering at North China University of Technology, Beijing, China.

His current research interest includes on predictive control of doubly fed induction generators and pulsewidth modulation rectifiers.

Jie Liu was born in 1992. He received the B.S. degree from the North China University of Technology, Beijing, China, in 2015, where he is currently working toward the M.S. degree in control science and engineering.

His research interests include control of pulsewidth modulation rectifiers.